Journal of Alloys and Compounds 513 (2012) 414–419

Contents lists available at SciVerse ScienceDirect

Journal of Alloys and Compounds

journal homepage: www.elsevier.com/locate/jallcom

High-performance $Li_3V_2(PO_4)_3$/C cathode materials prepared via a sol–gel route with double carbon sources

Lu-Lu Zhang[a,b], Ying Li[a], Gang Peng[b], Zhao-Hui Wang[a], Jun Ma[c,*], Wu-Xing Zhang[a], Xian-Luo Hu[a], Yun-Hui Huang[a,*]

[a] State Key Laboratory of Materials Processing and Die & Mould Technology, School of Materials Science and Engineering, Huazhong University of Science and Technology, Wuhan, Hubei 430074, China
[b] College of Mechanical and Material Engineering, Three Gorges University, 8 Daxue Road, Yichang, Hubei 443002, China
[c] School of Automotive Studies, Tongji University, Shanghai 201804, China

ARTICLE INFO

Article history:
Received 22 August 2011
Received in revised form 18 October 2011
Accepted 18 October 2011
Available online 25 October 2011

Keywords:
Lithium ion battery
Lithium vanadium phosphate
Sol–gel route
Double carbon sources
Electrochemical performance

ABSTRACT

$Li_3V_2(PO_4)_3$/C (LVP/C) composites have been successfully synthesized via an oxalic acid-based sol–gel process assisted by glucose, in which oxalic acid and glucose serve as double carbon sources. X-ray diffraction patterns show that all samples are well crystallized. Transmission electron microscopy images reveal that the LVP/C sample prepared with 15 wt% glucose is uniformly coated by carbon layer with an appropriate thickness of 8–10 nm, resulting in a high electrical conductivity and a fast kinetics. The Li^+-ion diffusion coefficient in the LVP/C sample prepared with glucose is $\sim 10^{-10}$ cm^2 s^{-1}, which is larger than that of the LVP/C sample prepared without glucose. The LVP/C sample prepared with 15 wt% glucose exhibits the best electrochemical performance with discharge capacity as high as 171 mAh g^{-1} at 0.1 C and 119 mAh g^{-1} at 10 C. The present work provides a valuable route for preparing lithium metal phosphates with double carbon sources to improve the conductivity and hence the electrochemical performance.
© 2011 Elsevier B.V. All rights reserved.

1. Introduction

Among the phosphate cathode materials, monoclinic $Li_3V_2(PO_4)_3$ (LVP) is promising for application since it shows high theoretical capacity (197 mAh g^{-1}), high operate voltage (average 4.0 V) and fast lithium ion migration resulting from its three-dimensional (3D) framework [1–4]. However, the intrinsic electronic conductivity of LVP is poor, which limits its practical application [2,4]. Many efforts have been done to enhance the conductivity, such as coating with carbon or metal [2,5–11] and doping with guest atoms [12–18]. Carbon coating is one of the most effective methods to improve the electronic conductivity. It can also prevent direct contact between LVP particles and electrolyte, which is helpful to alleviate dissolution of vanadium ions in the electrolyte [19]. To our knowledge, the effect of surface carbon depends greatly on carbon source. Up to now various carbon sources have been employed for carbon-coated LVP, such as glucose [8,20–24], sucrose [25], maltose [26,27], starch [20], humic acid [22], PVDF [20], polyvinyl alcohol [28,29], polyethylene glycol [30], carbon [7,11,22,31], stearic acid [32], citric acid [20,33], oxalic acid [34] and so on. The uniformity of carbon coating is crucial to achieve high electronic conductivity and Li^+-ion transfer. Double carbon sources have been recently used to improve the quality of carbon coating in $LiFePO_4$ [35].

Sol–gel method is very common to attain electrode materials with homogeneous morphology and uniform carbon layer. In the sol–gel process, oxalic acid is often used as chelating ligand, which can also act as carbon source and reducing agent. In this work, LVP/C composites were synthesized via oxalic acid-based sol–gel route assisted by glucose. Here, glucose served as the additional carbon source to modify the carbon-coated layer achieved by oxalic acid in LVP/C composites. The structure and electrochemical performance of the as-prepared LVP/C have been investigated.

2. Experimental

$Li_3V_2(PO_4)_3$/C composites were prepared via an improved sol–gel route with double carbon sources. All chemicals used were of analytical grade. Firstly, oxalic acid and V_2O_5 in stoichiometric molar ratio of 3:1 were dissolved in deionized water under stirring at 60 °C to achieve a clear blue solution. Secondly, stoichiometric $LiOH{\cdot}H_2O$ and $NH_4H_2PO_4$ were added into the solution in turn. The mixture was vigorously stirred at 60 °C to evaporate the water till a green gel was formed. The green gel was dried overnight at 80 °C in oven to obtain dry gel. The resulting gel was calcined at 350 °C for 6 h in N_2 and then cooled down to room temperature to achieve a precursor powder. Various amount of glucose (0, 10, 15, 20 wt% of the precursor powder) was added, and ball-milled with the precursor powder in ethanol for 2 h, followed by being dried at 60 °C for 12 h in air. The mixture was re-ground, and finally sintered at 700 °C for 10 h in N_2 to obtain final LVP/C samples. The samples prepared

* Corresponding authors. Tel.: +86 27 87558237; fax: +86 27 87558241.
E-mail addresses: huangyh@mail.hust.edu.cn (Y.-H. Huang), jun_ma@tongji.edu.cn (J. Ma).

0925-8388/$ – see front matter © 2011 Elsevier B.V. All rights reserved.
doi:10.1016/j.jallcom.2011.10.059

with 0, 10, 15 and 20 wt% of glucose are denoted as LVP/C0, LVP/C10, LVP/C15 and LVP/C20, respectively. The involved reactions can be expressed as below:

$$V_2O_5 + 3H_2C_2O_4 \rightarrow 2VOC_2O_4 + 2CO_2 + 3H_2O \quad (1)$$

$$2VOC_2O_4 + 3LiOH + 3NH_4H_2PO_4 + C_6H_{12}O_6 \rightarrow Li_3V_2(PO_4)_3 + 6C + 3CO_2 + CO + 3NH_3 + 12H_2O \quad (2)$$

X-ray diffraction (XRD) patterns were measured with an X'Pert Pro diffractometer (PANalytical B.V.) using Cu-K_α radiation (λ = 1.5406 Å). Morphologies of the samples were observed with scanning electron microscopy (SEM, Sirion 200, Holland). Carbon coating of the LVP/C powders was evaluated by transmission electron microscopy (TEM, Tecnai G2 20, Holland) and Raman spectra (VERTEX 70, Bruker). The content of the residual carbon was determined by carbon–sulfur analyzer (CS600, LECO, US).

The working electrodes were prepared by mixing active material with PVDF binder and acetylene black in a weight ratio of 75:15:10 in N-methyl pyrrolidinone solvent. The slurry of the mixture was coated on an aluminum foil (20 μm in thickness) using an automatic film-coating equipment. The resulting film was dried under an infrared light to remove volatile solvent, punched into discs (ϕ10 mm) and then pressed under a pressure of 6 MPa. The discs were transferred into an argon-filled glove box (Super 1220/750, Mikrouna) shortly after being dried at 120 °C for 12 h in vacuum. 2025 coin cells were assembled using Celgard 2300 as separator, lithium foil as counter and reference electrode. A solution of 1 mol l^{-1} $LiPF_6$ in a 1:1 (v/v) solvent mixture of ethylene carbonate and diethyl carbonate (EC/DEC) was employed as electrolyte. The cells were tested at various rates between 3.0 and 4.8 V at room temperature on a cell-testing instrument (LAND CT2001A, China). Cyclic voltammetry (CV) and electrochemical impedance spectra (EIS) measurements were performed on an electrochemical working station (PARSTAT 2273, Princeton Applied Research, America). CV curves were monitored at a scanning rate of 0.05 mV s^{-1} within a voltage range of 3.3–4.8 V, and EIS spectra were obtained over a frequency range from 1 MHz to 100 kHz after the first cycle.

3. Results and discussion

Fig. 1 shows the XRD patterns of the as-prepared LVP/C samples. The diffraction peaks for all samples are well indexed as monoclinic LVP with a space group of $P2_1/n$ (JCPDS No.: 80-1515). Only LVP/C0 contains some detectable impurity phases. Diffraction peaks of carbon have not been detected, indicating that the residual carbon is amorphous, or the carbon coating on LVP particles is too thin. Carbon contents of the LVP/C samples are listed in Table 1. Here, the

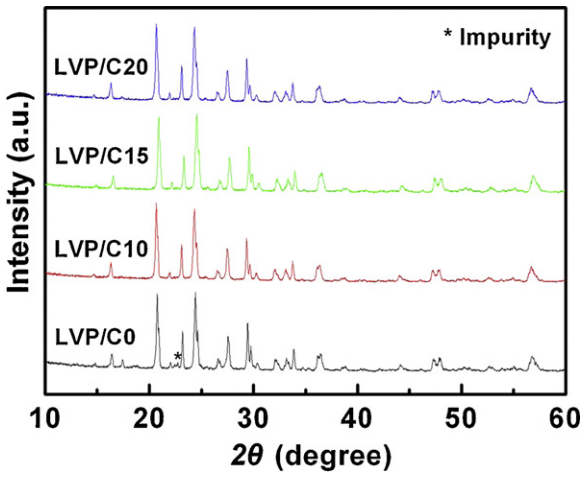

Fig. 1. XRD patterns for the as-prepared LVP/C samples.

residual carbon not only acts as a conductor to improve the electronic conductivity of LVP, but also forms a barrier to prevent the direct contact between LVP particles and the electrolyte, and hence minimizes the vanadium dissolution [19]. Obviously, the content of residual carbon in LVP/C0 prepared without additional glucose is the lowest (only 0.1%), resulting in few carbon coating and incomplete conversion of V^{5+}–V^{3+}. Thereby, it is necessary to provide additional carbon source to cover the shortage of residual carbon in the product obtained from stoichiometric oxalic acid and V_2O_5.

SEM images of samples are shown in Fig. 2. All samples present irregular agglomerated particles with obvious porous grain boundaries. The size for most particles is around several hundred nanometers. With increasing glucose content, there are some obvious additional species adhered to the particles, which is ascribed to the increasing residual carbon. TEM images are further used to investigate the influence of the additional glucose on microstructure for the LVP/C samples, as shown in Fig. 3. For LVP/C0 (Fig. 3a),

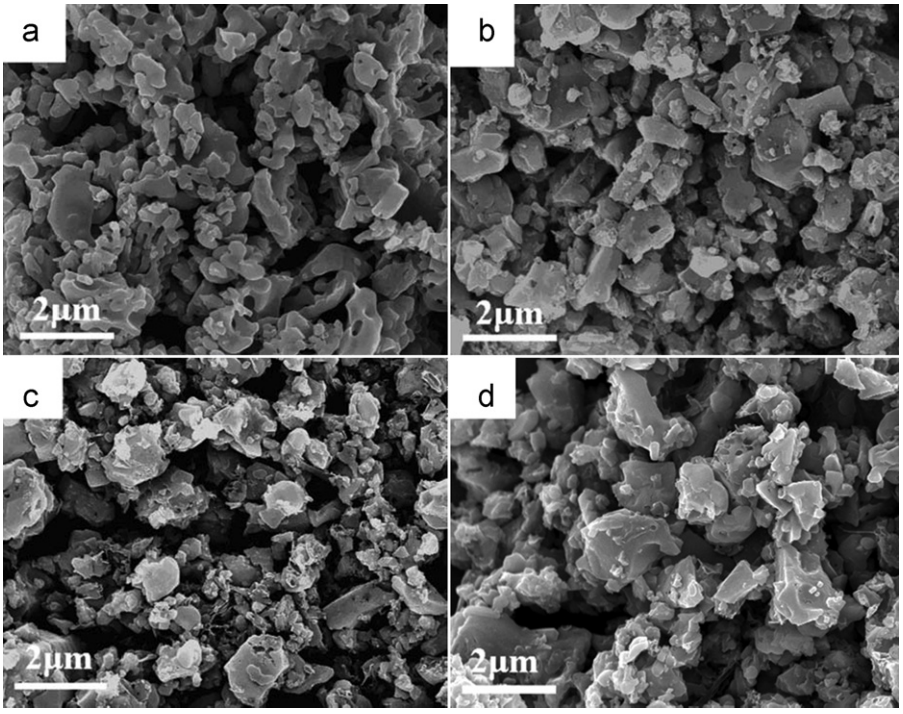

Fig. 2. SEM images of the LVP/C samples prepared with different glucose amount, (a) LVP/C0, (b) LVP/C10, (c) LVP/C15 and (d) LVP/C20.

Table 1
Carbon content, capacity, capacity retention, Li^+ diffusion coefficient, I_D/I_G and charge-transfer resistance (R_{ct}) for $Li_3V_2(PO_4)_3$/C samples.

Sample	LVP/C0	LVP/C10	LVP/C15	LVP/C20
Carbon content (wt%)	0.10	2.20	3.19	4.25
1st discharge capacity (mAh g^{-1})	145	162	171	159
50th discharge capacity (mAh g^{-1})	108	135	139	128
Capacity retention (%)	74.3	83.6	81.1	80.8
D_{Li+} (cm^2 s^{-1})	4.20×10^{-11}	1.34×10^{-10}	3.72×10^{-10}	2.50×10^{-10}
I_D/I_G	–	1.32	1.22	1.20
R_{ct} (Ω)	811.5	772.3	573.7	694.4

no obvious carbon coating is found on the particle surface, but adhesion phenomenon is observed. For LVP/C20 (Fig. 3d), multilayer carbon coating with irregular shape tightly wraps around the LVP particles. Typical core–shell structures are observed in the images of LVP/C10 and LVP/C15 (Fig. 3b and c). *In situ* generated pyrolytic carbon is more beneficial for forming a continuous coating. The thickness of carbon coating agrees well with the content of residual carbon in Table 1. The more the residual content, the thicker the carbon coating is. The 8–10 nm thickness of carbon coating on the surface of LVP/C15 is more appropriate for forming an ideal conducting network to enhance conductivity and alleviate vanadium dissolution, resulting in a faster lithium ion transfer and better electrochemical performance.

Fig. 4 shows the initial charge/discharge curves and cycle performances for the LVP/C cathode materials. As shown in Fig. 4a, all electrodes clearly present four charge plateaus around 3.61, 3.70, 4.10 and 4.56 V, which is the characteristic of two phase behavior between the single phase of $Li_xV_2(PO_4)_3$ with $x = 3.0$, 2.5, 2.0, 1.0 and 0 [3]. In the discharge process, the characteristic S-shaped curve corresponds to a solid solution behavior, whereas two subsequent electrochemical plateaus demonstrate the reinsertion of the last Li^+ from $Li_2V_2(PO_4)_3$ to $Li_{2.5}V_2(PO_4)_3$ and then to $Li_3V_2(PO_4)_3$. With increasing glucose, the charge plateaus shift downward and become wider, whereas the discharge plateaus shift upward, indicating that polarization between charge and discharge is somewhat suppressed with addition of glucose. As seen in Fig. 4b, discharge capacity is also remarkably improved after adding glucose. For LVP/C0, it only delivers a discharge capacity of 145 mAh g^{-1} with a coulombic efficiency of 85.9% at 0.1 C, and the discharge capacity fades down to 108 mAh g^{-1} after 50 cycles. LVP/C15 delivers the highest capacity of 171 mAh g^{-1} with coulombic efficiency of 88.2%, and keeps a discharge capacity of 139 mAh g^{-1} even after 50 cycles. The residual carbon content in LVP/C15 is 3.19%, which is adequate to form an effective carbon coating and hence to provide good conducting network for the kinetic extraction/insertion reaction of Li^+ ions. It is noted that the capacity retention decreases with increasing additional glucose, though the capacity retention of all LVP/C samples with glucose is higher than that of LVP/C0. The capacity loss can be ascribed to the unconverted inactive LVP at the center of the particle or the trapped isolated zones of LVP. In the present case, the enlarged transmission path for lithium ions and electrons caused by thick carbon coating may lead to additional capacity loss for LVP/C samples.

We further compare the discharge profile and rate capability between LVP/C0 and LVP/C15 electrodes in Fig. 5. The cells were charged at 0.1 C and discharged at different C-rate ranging from 0.5 to 10 C each for ten cycles. With increasing current density, the discharge capacity decreases for LVP/C0 and LVP/C15 cathodes, and the characteristic S-shaped curves during the initial discharge process and the two subsequent electrochemical plateaus (i.e. 3.6 V and 3.5 V) gradually disappear (see Fig. 5a). Nevertheless, the discharge capacity of the LVP/C15 composite cathode still reaches

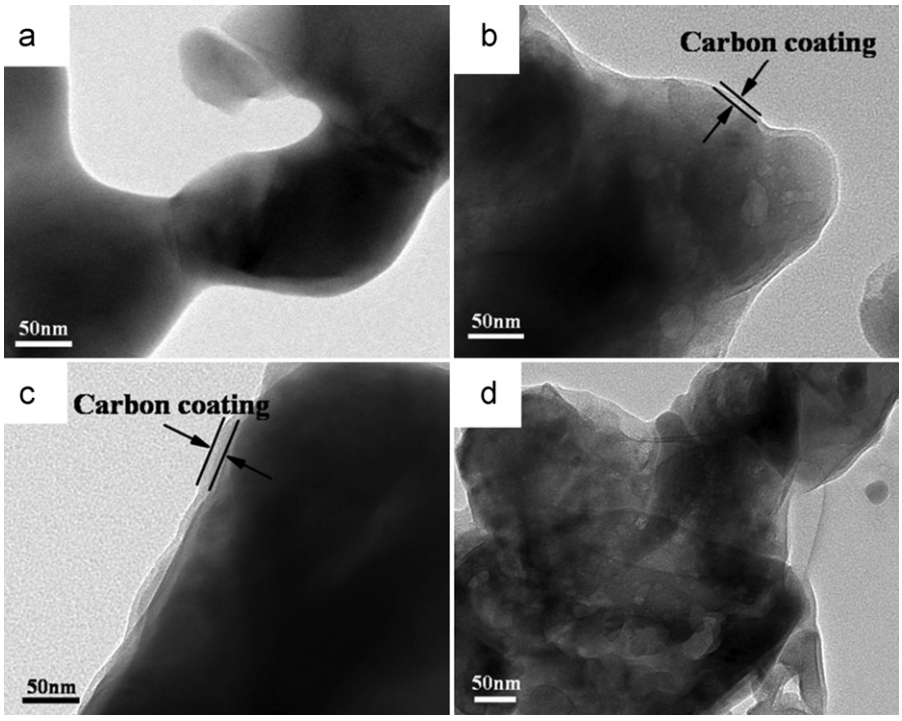

Fig. 3. TEM images of the LVP/C samples prepared with different glucose amount, (a) LVP/C0, (b) LVP/C10, (c) LVP/C15 and (d) LVP/C20.

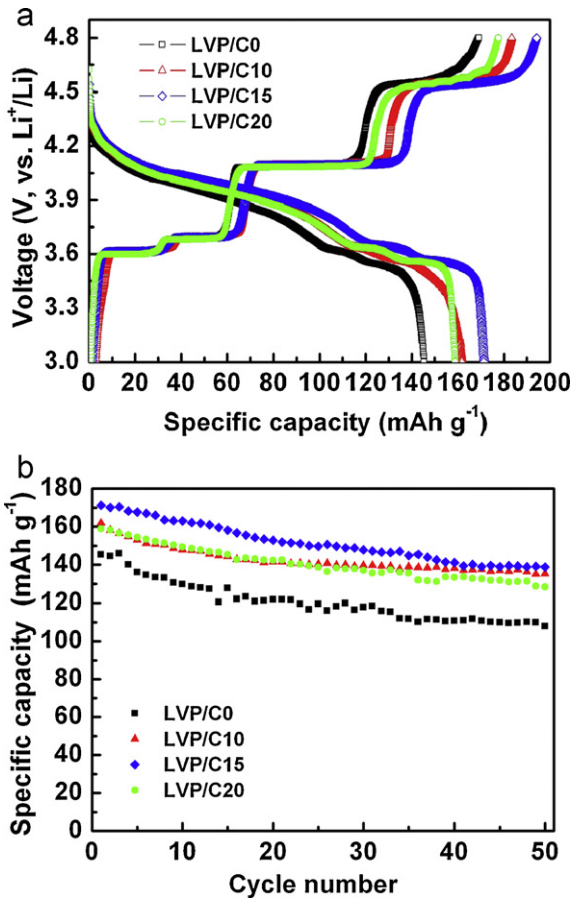

Fig. 4. (a) Initial charge/discharge profiles and (b) cycle performance for the prepared LVP/C electrodes at 0.1 C.

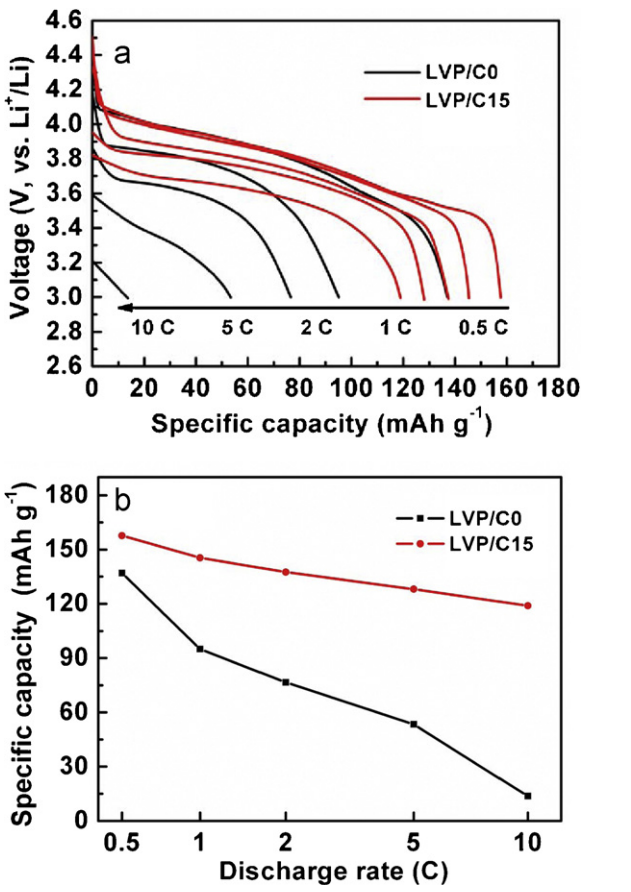

Fig. 5. (a) Discharge profiles and (b) rate capability for LVP/C0 and LVP/C15 at C-rate varying from 0.5 C to 10.0 C each for 10 cycles.

128 mAh g^{-1} at 5 C and 119 mAh g^{-1} at 10 C. For LVP/C0 cathode, only 53 mAh g^{-1} at 5 C and 14 mAh g^{-1} at 10 C are obtained. The rate capability for LVP/C15 is significantly enhanced as compared with LVP/C0.

Fig. 6 shows cyclic voltammetry curves of LVP/C electrodes at a scanning rate of 0.05 mV s^{-1} between 3.3 and 4.8 V. With additional glucose, the redox peaks become sharp and well-shaped. Four anodic peaks around 3.6 V, 3.7 V, 4.1 V, 4.6 V and three cathodic peaks around 3.9 V, 3.6 V, 3.5 V clearly appear, which agrees well with the charge–discharge curve in Fig. 4a. In the initial Li^+ reinsertion process, a wide cathodic peak at 3.9 V corresponds to the S-shaped galvanostatic discharge curve, indicative of solid solution behavior. Obviously, the anodic peak current at 4.6 V is the lowest, which is ascribed to the extraction of the third lithium ion. Therefore, extraction of the third lithium ion is kinetic control step due to the reduced ionic/electronic conductivity of the fully extracted phase $V_2(PO_4)_3$ [3]. The relationship between the peak current and Li^+ diffusion can be explained with the Randles Sevcik equation [36]:

$$I_p = 2.69 \times 10^5 n^{3/2} A D^{1/2} v^{1/2} C \quad (3)$$

where I_p is the CV peak current (A), n is the number of electrons involved in the redox process, A is the electrode area (cm^2), D is the Li^+ diffusion coefficient ($cm^2\ s^{-1}$), v is the potential scan rate ($V\ s^{-1}$), and C is the concentration of lithium ions in the cathode ($mol\ cm^{-3}$). The lower CV peak current, the lower the Li^+-ion diffusion coefficient is. Here, a_4 peak is used to calculate the Li^+-ion diffusion coefficient. Basing on Eq. (3), Li^+ diffusion coefficients in LVP/C samples prepared with different glucose (0, 10, 15 and 20 wt%) are calculated to be 4.20×10^{-11}, 1.34×10^{-10}, 3.72×10^{-10} and $2.50 \times 10^{-10}\ cm^2\ s^{-1}$, respectively (Table 1). LVP/C0 shows the lowest Li^+ diffusion coefficient, corresponding to the highest over-potential during the lithium extraction/insertion process. LVP/C15 exhibits the highest Li^+ diffusion coefficient, indicative of an enhancement of reversibility in the electrode reaction.

Fig. 7 displays Raman spectra of the as-prepared LVP/C samples with different glucose. For LVP/C0, no sharp D peak (~1310 cm^{-1}) and G peak (~1600 cm^{-1}) is found in its Raman spectrum, which is due to the low residual carbon. For the LVP/C samples prepared with glucose (i.e. LVP/C10, LVP/C15 and LVP/C20), strong D peak and G peak appear in the Raman spectra. The lower the D/G

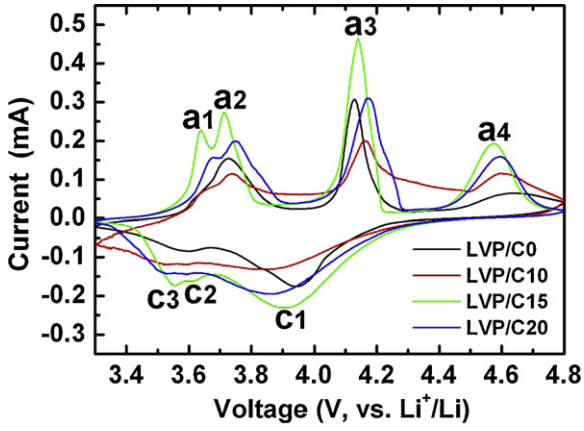

Fig. 6. CV curves within potential range of 3.3–4.8 V (vs. Li^+/Li) at scanning rate of 0.05 mV s^{-1} for the LVP/C composites.

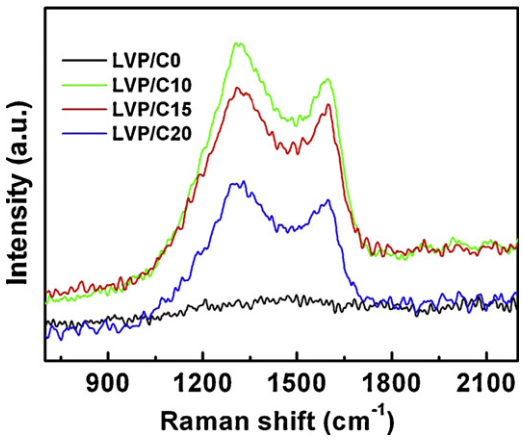

Fig. 7. Raman spectra for the LVP/C samples prepared with different glucose amount.

intensity ratio, the higher the electrical conductivity is. As seen in Table 1, the more the residual content, the lower the integrated D/G intensity ratio of Raman is. Wilcox et al. [37] pointed out that the D/G intensity ratio is useful to compare samples with each other but it is not a quantitative value to determine the disordered carbon or graphene contents; they found that the D/G ratio decreased as more carbon source pyromellitic acid was added. In our work, the D/G ratios of LVP/C15 and LVP/C20 are very close, but both are lower than that of LVP/C10, which indicates that LVP/C15 and LVP/C20 exhibit higher electrical conductivity. Furthermore, small intensity ratio of PO_4^{3-} (953 cm^{-1}) and carbon bands for LVP/C10, LVP/C15 and LVP/C20 demonstrate that carbon coating on the surface of their particles is uniform. High conductivity and uniform coating facilitate the kinetic process of the electrochemical reactions.

The Nyquist plots for the LVP/C cells are shown in Fig. 8. Considering the penetration of electrolyte into the electrode, structural change and solid electrolyte interphase (SEI) formation of electrode [38], we choose the second cycle for comparison. The EIS spectra for the four samples look very similar, which consist of a very small intercept at high frequency, a depressed semicircle at high-to-medium frequency and an inclined line at low frequency. The insert of Fig. 8 shows the equivalent circuit composed of "R(C(RW))" assembled in series by fitting the EIS spectra with the ZSimpWin program. R_C represents bulk resistance of the cell, which corresponds to the small intercept. R_{ct} and C_{dl} are, respectively, the charge-transfer resistances at the electrode/electrolyte interface and the double-layer capacitance between the electrolyte and cathode, which correspond to the depressed semicircle. Z_W is the Warburg impedance related to the diffusion of lithium ions within

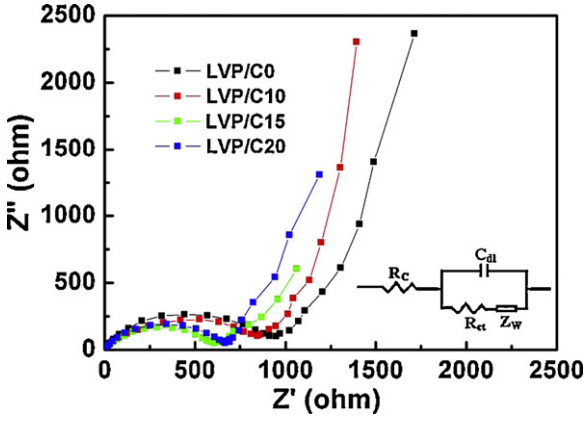

Fig. 8. EIS spectra of the as-prepared LVP/C unit cells after first cycle.

the electrode, which corresponds to the inclined line. Low charge-transfer resistance (R_{ct}) corresponds to a fast kinetics of the Faradic reaction. As listed in Table 1, R_{ct} values of LVP/C samples with additional glucose as carbon source are lower than that of LVP/C0, indicative of better conducting network in the glucose-achieved LVP/C samples. It is noted that R_{ct} at first decreases with increasing glucose amount, then increases when the amount of glucose is up to 20 wt%. It can be inferred that the excessive residual carbon can easily form a thick carbon coating to prevent the transition of charge, which agrees well with the polarization phenomenon in Fig. 4a. Therefore, the LVP/C sample obtained with appropriate amount of glucose as the second carbon source can exhibit excellent electrochemical performance due to good conducting network and uniform carbon coating.

4. Conclusions

LVP/C composites have been successfully synthesized via a sol–gel process with chelating agent oxalic acid and glucose as double carbon sources. The electrochemical performances of the LVP/C composites are remarkably improved with addition of glucose. The optimized LVP/C sample with 15% glucose shows a discharge capacity as high as 171 mAh g^{-1} at 0.1 C and 119 mAh g^{-1} at 10 C, indicative of high capacity and excellent rate capability. Our experiments reveal that addition of glucose as second carbon source gives rise to uniform carbon coating with an appropriate thickness, resulting in high electrical conductivity and large Li^+ diffusion coefficient. Therefore, for preparation of the cathode materials with poor intrinsic electronic transport such as lithium metal phosphates, it is helpful to use double carbon sources to form coated carbon layer with high quality to achieve superior electrochemical performance.

Acknowledgements

This work was supported by the NSFC (Grant nos. 50825203 and 21175050) and the MOST of China (Grant nos. 2009AA03Z225 and 2010DFB70090). In addition, the authors thank the Analytical and Testing Center of Huazhong University of Science and Technology for providing XRD, SEM, TEM and Raman spectra measurements.

References

[1] M.Y. Saïdi, J. Barker, H. Huang, J.L. Swoyer, G. Adamson, Electrochem. Solid State Lett. 5 (2002) A149.
[2] H. Huang, S.C. Yin, T. Kerr, N. Taylor, L.F. Nazar, Adv. Mater. 14 (2002) 1525.
[3] S.C. Yin, H. Grondey, P. Strobel, M. Anne, L.F. Nazar, J. Am. Chem. Soc. 125 (2003) 10402.
[4] L.L. Zhang, X. Zhang, Y.M. Sun, W. Luo, X.L. Hu, X.J. Wu, Y.H. Huang, J. Electrochem. Soc. 158 (2011) A924.
[5] X.H. Rui, Y. Jin, X.Y. Feng, L.C. Zhang, C.H. Chen, J. Power Sources 196 (2011) 2109.
[6] P. Fu, Y. Zhao, Y. Dong, X. An, G. Shen, J. Power Sources 162 (2006) 651.
[7] Y. Li, Z. Zhou, M. Ren, X. Gao, J. Yan, Electrochim. Acta 51 (2006) 6498.
[8] C. Chang, J. Xiang, X. Shi, X. Han, L. Yuan, J. Sun, Electrochim. Acta 54 (2008) 623.
[9] Y.Q. Qiao, X.L. Wang, Y. Zhou, J.Y. Xiang, D. Zhang, S.J. Shi, J.P. Tu, Electrochim. Acta 56 (2010) 510.
[10] L. Zhang, X.L. Wang, J.Y. Xiang, Y. Zhou, S.J. Shi, J.P. Tu, J. Power Sources 195 (2010) 5057.
[11] A. Pan, J. Liu, J.-G. Zhang, W. Xu, G. Cao, Z. Nie, B.W. Arey, S. Liang, Electrochem. Commun. 12 (2010) 1674.
[12] M. Ren, Z. Zhou, Y. Li, X.P. Gao, J. Yan, J. Power Sources 162 (2006) 1357.
[13] T. Jiang, Y.J. Wei, W.C. Pan, Z. Li, X. Ming, G. Chen, C.Z. Wang, J. Alloys Compd. 488 (2009) L26.
[14] Y. Chen, Y. Zhao, X. An, J.Y. Dong, L. Chen, Electrochim. Acta 54 (2009) 5844.
[15] Y.G. Mateyshina, N.F. Uvarov, J. Power Sources 196 (2011) 1494.
[16] C. Dai, Z. Chen, H. Jin, X. Hu, J. Power Sources 195 (2010) 5775.
[17] J.S. Huang, L. Yang, K.Y. Liu, Y.F. Tang, J. Power Sources 195 (2010) 5013.
[18] Q. Kuang, Y. Zhao, X. An, J. Liu, Y. Dong, L. Chen, Electrochim. Acta 55 (2010) 1575.
[19] S. Patoux, C. Wurm, M. Morcrette, G. Rousse, C. Masquelier, J. Power Sources 119–121 (2003) 278.

[20] X.H. Rui, C. Li, C.H. Chen, Electrochim. Acta 54 (2009) 3374.
[21] L. Wang, L.C. Zhang, I. Lieberwirth, H.W. Xu, C.H. Chen, Electrochem. Commun. 12 (2010) 52.
[22] X. Zhou, Y. Liu, Y. Guo, Electrochim. Acta 54 (2009) 2253.
[23] M.M. Ren, Z. Zhou, X.P. Gao, W.X. Peng, J.P. Wei, J. Phys. Chem. C 112 (2008) 5689.
[24] L. Wang, X. Zhou, Y. Guo, J. Power Sources 195 (2010) 2844.
[25] S. Zhong, J. Wang, L. Liu, J. Liu, Y. Li, Ionics 16 (2010) 117.
[26] X.H. Rui, N. Ding, J. Liu, C. Li, C.H. Chen, Electrochim. Acta 55 (2010) 2384.
[27] X.H. Rui, C. Li, J. Liu, T. Cheng, C.H. Chen, Electrochim. Acta 55 (2010) 6761.
[28] T. Jiang, W.C. Pan, J. Wang, X.F. Bie, F. Du, Y.J. Wei, C.Z. Wang, G. Chen, Electrochim. Acta 55 (2010) 3864.
[29] J. Wang, X. Zhang, J. Liu, G. Yang, Y. Ge, Z. Yu, R. Wang, X. Pan, Electrochim. Acta 55 (2010) 6879.
[30] J. Wang, J. Liu, G. Yang, X. Zhang, X. Yang, X. Pan, R. Wang, Electrochim. Acta 54 (2009) 6451.
[31] Y.Q. Qiao, J.P. Tu, Y.J. Mai, L.J. Cheng, X.L. Wang, C.D. Gu, J. Alloys Compd. 509 (2011) 7181.
[32] Y.Q. Qiao, X.L. Wang, J.Y. Xiang, D. Zhang, W.L. Liu, J.P. Tu, Electrochim. Acta 56 (2011) 2269.
[33] F. Yu, J. Zhang, Y. Yang, G.Z. Song, J. Solid State Electrochem. 14 (2010) 883.
[34] J.C. Zheng, X.H. Li, Z.X. Wang, S.S. Niu, D.R. Liu, L. Wu, L.J. Li, J.H. Li, H.J. Guo, J. Power Sources 195 (2010) 2935.
[35] S.W. Oh, S.-T. Myung, S.-M. Oh, K.H. Oh, K. Amine, B. Scrosati, Y.-K. Sun, Adv. Mater. 22 (2010) 4842.
[36] J.R. Dahn, J.W. Jiang, L.M. Moshurchak, J. Electrochem. Soc. 152 (2005) A1283.
[37] J.D. Wilcox, M.M. Doeff, M. Marcinek, R. Kostecki, J. Electrochem. Soc. 154 (2007) A389.
[38] M.V. Reddy, B. Pecquenard, P. Vinatier, A. Levasseur, Electrochem. Commun. 9 (2007) 409.